

Inter- and Transgranular Nucleation and Growth of Voids in Shock Loaded Copper Bicrystals



Elizabeth Fortin, Benjamin Shaffer, Saul Opie, Matthew Catlett and Pedro Peralta

Abstract Understanding the evolution of dynamic deformation and damage due to spall at grain boundaries (GBs) can provide a basis for connecting micro- to macroscale failure behavior in polycrystalline metals undergoing extreme loading conditions. Bicrystal samples grown from the melt were tested using flyer-plate impacts with shock stresses from 3 to 5 GPa. Pulse duration and crystal orientation along the shock direction were varied for a fixed boundary misorientation to determine thresholds for void nucleation and coalescence in both the bulk and the boundary. Sample characterization was performed using electron backscattering diffraction (EBSD) and scanning electron microscopy (SEM) to gather microstructural information at and around the GB, with emphasis on damage at the boundary. Simulations were performed to interpret experimental results. Initial results show that the kinetics of damage growth at the boundary is strongly affected by pulse duration and stress level and that once a threshold level is reached, damage increases faster at the GB compared to the grain bulks.

Keywords Spall · Bicrystal · Pulse duration · Grain boundary

Introduction

Shock loading is a dynamic condition that can lead to material failure and deformation starting at the microstructural level such as cracking, void nucleation and growth, and eventually spallation, the most common failure mode [1]. The amount of spall observed in a sample can vary with loading conditions, e.g. pressure and

E. Fortin (✉) · B. Shaffer · P. Peralta
Arizona State University, Tempe, AZ, USA
e-mail: evfortin@asu.edu

S. Opie
General Atomics, Palmdale, CA, USA

M. Catlett
Los Alamos National Laboratory, Los Alamos, NM, USA

© The Minerals, Metals & Materials Society 2019
B. Li et al. (eds.), *Characterization of Minerals, Metals, and Materials 2019*, The Minerals, Metals & Materials Series,
https://doi.org/10.1007/978-3-030-05749-7_11

pulse duration [1–3]. Previous research has determined that the microstructure does play an important role in damage nucleation and growth, through parameters such as grain size [3, 4], grain boundaries [5–9], the effects of which are compounded by material anisotropy [2]. By studying the deformation patterns at and around GBs in samples where damage in its incipient or intermediate stages, we can determine preferential sites in the material's microstructure where voids will nucleate and grow. The observation of spall damage on a material is important because if a structure is impacted at a high enough pressure for fracture to occur, there is a possibility that microstructural cracks can grow to the macroscale leading the structure to burst from the inside out. The purpose of this work is to understand the kinetics of void nucleation and growth at selected grain boundaries using copper bicrystals to have a single boundary that allows for the sole observance of the effect at the boundary without other interactions.

Experiments on copper multicrystals performed by Peralta et al. [5] have proved that some grain boundaries have a stronger response to dynamic loading than others. Results showed that tips of terminated twins, which are the high energy and mobility ends of an annealing twin with an incoherent boundary [5], were the sites of damage localization in many of the copper samples. Work performed by Wayne et al. [10] found that terminated twins and grain boundaries with misorientation angles between the 25° and 60° range were preferred sites for intergranular damage nucleation. Shock loading experiments were also performed on copper samples with different thermomechanical histories (heat treated, fully recrystallized, and as received), producing grain size and plastic deformation variations in [11, 12]. Results confirmed previous findings of Wayne et al. [10] that the 25°–50° range is favorable for damage nucleation, regardless of the initial conditions, and that damage was unlikely to nucleate at {111} Σ 3 boundaries. The work suggests that plasticity in the grain bulks is responsible for the incipient spall to nucleate at the weaker grain boundaries in the microstructure [11, 12]. Escobedo et al. [13] found in spalled tantalum samples that damage occurred at low coincidence, high angle grain boundaries. Subsequent work performed by Cerreta et al. in [7] where they concluded that 3 and low-angle boundaries were resistant to void nucleation with peak compressive stresses between 1.5 and 2.5 GPa during shock loading. This further confirmed the earlier results found by Wayne et al. [10].

The effect of pulse shape has been reported in work performed by Gray et al. [14] on 316L stainless steel using Taylor waves, or triangular-shaped, and square-topped pulse shapes. Peak shock stresses were 6.6, 10.2, and 14.5 GPa. The triangular-shaped pulse showed damage only at 14.5 GPa, while results for the square pulse showed incipient spallation at 6.6 GPa. From this, it can be seen that the square-shaped pulse has a lower spall strength than the triangular pulse. Pulse duration was also explored by Gray et al. [15] using three different pulse durations, 0.84, 0.28, and 0.25 μ s on Tantalum targets, reaching peak stresses of 7.4, 10.6, and 21 GPa, respectively. Different flyer thicknesses, 2.25, 2.42, and 6.25 mm, were used to vary pulse duration, while target thickness remained constant at 4.572 mm. The 21 GPa sample resulted in full spallation, with a scab being ejected from the free surface,

with the 7.4 and 10.6 GPa samples show incipient spallation. From this, it can be seen that a longer pulse duration and higher peak shock stress create more damage.

Molecular dynamic simulations have been performed Rudd and Belak [16] in order to study void nucleation and growth. Results showed that GBs are the preferential sites for void nucleation and void growth is anisotropic [16]. Molecular dynamic simulations of copper bicrystals performed by An et al. [9] found that most of the damage still takes place in the GB region due to boundary weakening. Secondary void nucleation was also found to be more pronounced in the grain that had more activated slip systems. This difference in damage is attributed to differences in plastic deformation, caused by the structural asymmetry of the grain boundary [9]. Wilkerson et al. [17] have studied the dislocation kinetics on dynamic void growth using a dislocation-based viscoplastic computational model. They discovered that dislocation kinetics and micro-inertia effects play a role in dynamic void growth. It was found that micro-inertia affected void growth once the void was larger than a micron, and the growth of smaller voids was dominated by dislocation kinetics. The authors also state that smaller grains can cause a lower spall strength by inversely following the Hall–Petch behavior. The fast nature of shock loading does not allow dislocation movement to be the dominant failure mode; instead, failure will occur at the weak point of the sample, the grain boundaries.

In this study, SEM and EBSD were used alongside optical microscopy (OM) to observe the damage at the GB and grain bulks to understand the roles pulse duration and crystal orientation play in void nucleation and growth at individual boundaries.

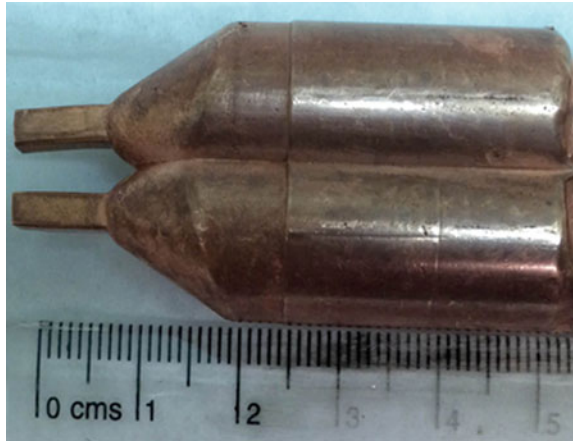
Materials and Methods

Bicrystal Growth

Bicrystals were grown using a modified vertical Bridgman technique [18]. A graphite mold was constructed to fit inside a quartz tube and to hold the single crystal seeds and stock copper. The graphite mold used has reentrant corners that pinned the boundary so that it is located where both the single crystals meet (see [18]). The mold also had a bottom hole where a thermocouple is located to measure the temperature of the seed. The temperature profile of the furnace used was measured so the seeds would be placed just below the hottest zone of the furnace. This way, once the top portion of the seeds reached melting temperature, the stock copper placed on the top was already molten, allowing for the seed orientation to quickly grow upwards once the temperature in the furnace is reduced by decreasing the power.

A thermolyne furnace model 21100 was used for the bicrystal growth. The system was purged with UHP Argon gas for 10 min prior to starting the experiment. The furnace was consistently ramped up by increasing the set point 300 °C at a time until the thermocouple monitoring the seed temperature approached 1080 °C. The set point of the furnace was then increased by 1° at a time until the inner thermocouple

Fig. 1 Bicrystal boule after growth



read 1083 °C. The furnace was held at 1083 °C for 10 min to allow for enough time to melt the full load of material inside the mold. Then, the furnace set point was increased a degree until the inner thermocouple read 1084 °C, the furnace was held there for 30 s. This process allows for the seeds to slightly melt, which results in the seed orientation growing vertically along the mold, producing a bicrystal. Then, the setpoint of the furnace was decreased by 1° a minute for the first 20° and 2° a minute for the next 40°. The resulting boule is shown in Fig. 1.

Sample Preparation

Samples were sectioned from the resulting bicrystals via electro-discharge machining (EDM) and polished to their desired thicknesses. The sample surfaces were finished with 0.02 μm colloidal silica and a planarity of 0.05°. Two different configurations of bicrystal samples were studied in order to understand the effect of crystal orientation on the damage kinetics for a fixed grain boundary misorientation. Targets were fabricated from the parallel, or growth direction, and perpendicular directions on the bicrystal boule. The crystallography of both targets is shown in Fig. 2. The grains are labeled 1 and 2 in the inverse pole figures to correspond to the orientations shown in the EBSD scan for both the growth and punch out directions. Figure 3 shows where samples were extracted from the boule.

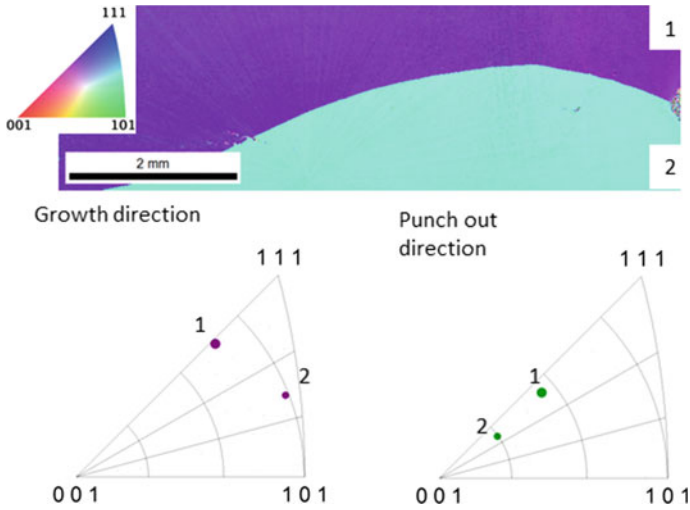


Fig. 2 Top: EBSD scan of the undeformed growth direction, bottom: inverse pole figures for the growth and punch out directions

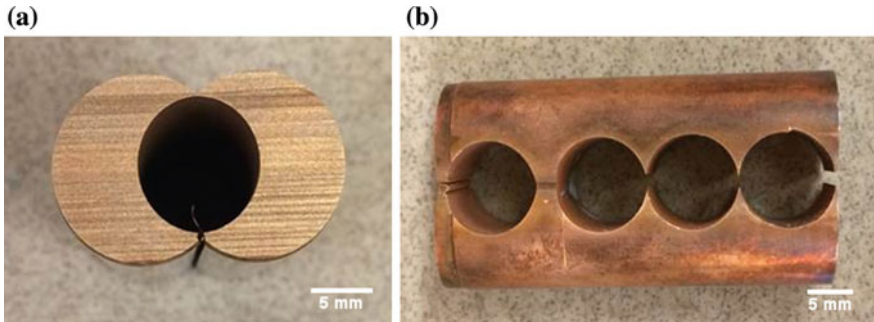


Fig. 3 **a** Growth direction cut, **b** punch out direction cut

Flyer-Plate Impact

Flyer-plate impacts were performed on a light gas gun system at ASU. Bicrystal targets measured 10 mm in diameter and 1 mm thick, while copper polycrystals flyers were 8 mm in diameter and either 500, 385, or 225 μm thick. The flyer was attached to an ultra-high molecular-weight polyethylene sabot using epoxy. The sabot had a hole machined in the center, which gave the flyer a free surface on the backside and provided an alignment tool to place the flyer in the center of the sabot face. Targets were placed in a PMMA window with a hole machined in the center to give the backside of the target a free surface. The target and window were placed in a PMMA holder and secured in the recovery chamber of the gas gun. The sabot is

launched down the barrel of the gas gun via a light gas, such as nitrogen. Shortly after exiting the barrel, the flyer attached to the sabot will come into contact with the target in the recovery chamber. Growth direction sample velocities began at 200 m/s and increased by 10 m/s until 240 m/s, while punch out sample velocities began at 225 m/s and increase by 5 m/s until 240 m/s. Maximum pressures ranged from 3.7 to 4.5 GPa. The velocities were chosen based off of previous experiments where incipient and intermediate, or coalescence, spallation was observed at the boundary. Intermediate spallation was seen at the boundary in both targets at 240 m/s, while incipient spall was seen at the boundary at 200 m/s for the growth direction targets and 225 m/s for the punch out direction targets.

The gas gun uses a laser/photodiode/oscilloscope system to capture the velocity of the flyer before impact. A laser beam passes directly through the recovery chamber and meets the photodiode on the opposite side, which is attached to an oscilloscope, where data is captured. As the projectile leaves the barrel and crosses the laser beam, the oscilloscope is triggered to record the change of light the photodiode experiences. From the result recorded on the oscilloscope, time is measured from where the signal begins to drop to where the signal begins to rise, left to right. Then, velocity can be calculated by dividing the length of the projectile by the time spent passing the laser beam. The resulting velocity measurements are, approximately ± 1.6 m/s accurate. This initial velocity data is enough information to determine the maximum shock stress experienced by the sample.

Post-Shot Characterization

After the experiment, targets were soft recovered and cross-sectioned so that the boundary was perpendicular to the cut. The cross sections were then polished to EBSD quality and scanned to observe the spall damage at the boundary and within the bulk of the grains. Consecutive sectioning was also performed through the thickness of the spall zone to observe the change in the void nucleation and growth at the boundary.

Abaqus Simulations

A dynamic, explicit Abaqus model and crystal plasticity subroutine based on the model described in [19] to simulate flyer-plate impact. An 8 mm in diameter flyer and a 10 mm in diameter target with the desired thicknesses were used to match the samples used in gas gun experiments. The target was partitioned in half and a separate crystallographic orientation was assigned to each half as determined from EBSD data collected on the as grown bicrystals. The flyer was assigned a predefined velocity field and set to the measured impact velocity during the experiment. Figure 4 shows the flyer-plate model.

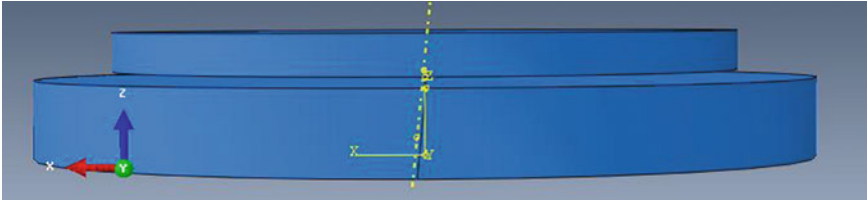


Fig. 4 Flyer-plate model used for simulations. The flyer is on top and the partitioned target is below

The crystal plasticity subroutine used [19] is specialized to FCC materials and uses a multiplicative decomposition of the deformation gradient that includes a volumetric component to account for damage due to void nucleation and growth, as follows:

$$F = F_e F_v F_p \quad (1)$$

where F is the total deformation gradient, F_e is the elastic part of the deformation, F_v is the volumetric part of the deformation due to void nucleation and growth, and F_p is the isochoric plastic deformation [20, 21]. Damage due to void growth and nucleation is accounted for using a Gurson–Tvergaard–Needleman (GTN) model where the voids are assumed to grow isotropically and micro-inertia effects can be ignored when observing void nucleation at an incipient stage [22]. Further information about the crystal plasticity subroutine used in this work can be found in [19].

Results and Discussion

Bicrystal Growth Results

After the boule is recovered, the seeds are removed and a small sliver of the boule is cut to verify that only two grains exist. The boundary is naturally meandering, shown in Fig. 2, so that it makes a good surrogate for boundaries found in actual polycrystals and multicrystals, which have curvature as well. The misorientation measured 42° across the boundary, which was found to be close to the misorientation most likely to nucleate damage from results in [4, 12].

Shot Conditions

Results from the flyer-plate impact experiments are shown in Tables 1 and 2 for the growth and punch out direction shots, respectively. Results are shown for the samples

Table 1 Growth direction shot conditions

Flyer thickness (μm)	Shot number	Velocity (m/s)	σ_{max} (GPa)	Left grain damage	Boundary damage	Right grain damage
225	122	233.7	4.29	Incipient	None	None
	127	240.1	4.42	Incipient	None	Incipient
385	121	199.7	3.65	Incipient	Incipient	Incipient
	119	230.6	4.23	Incipient	Coalesced	Incipient
	117	240.3	4.42	Incipient	Coalesced	Incipient
500	110	223.4	4.1	Incipient	Incipient/ coalesced	Incipient
	112	232.6	4.27	Incipient	Coalesced	Incipient

Table 2 Punch out direction shot conditions

Flyer thickness (μm)	Shot number	Velocity (m/s)	σ_{max} (GPa)	Left grain damage	Boundary damage	Right grain damage
385	148	230.7	4.24	None	Incipient	Incipient
	151	240.7	4.43	None	Unzipped	None
500	159	227.5	4.17	Incipient	Unzipped	Incipient
	136	239.4	4.4	Incipient	Unzipped	Incipient

that did nucleate damage and are grouped by flyer thickness (225, 385, 500 μm) and velocity. Damage at the boundary and each bulk were also recorded.

Gas Gun Experiments

From both the growth and punch out direction results, the 225 μm flyers were unable to nucleate damage at the boundary. In the growth direction shots 122 and 127, damage was observed in the bulk of the grains, indicating that the boundary was stronger than the bulks for short pulses at high velocities. However, no damage was observed in the punch out samples with similar velocities (shots 156 and 150), showing how the difference in orientation affects strength. The boundary also behaves differently between the growth and punch out samples. For the 385 μm flyer shots, the growth direction boundary shows an incipient coalescence at 213.1 m/s (shot 191), while coalescence is not observed until 240 m/s (shot 151) in the punch out direction.

Taylor Factor maps for both the growth and punch out directions are shown in Figs. 5 and 6, respectively. The Taylor Factors from the figures from top to bottom are 3.24 and 3.42 for the growth direction and 2.94 and 2.37 for the punch out



Fig. 5 Taylor factor map of the growth direction



Fig. 6 Taylor factor map of the punch out direction

direction. The punch out direction has the higher Taylor Factor mismatch between the two grains with 0.57. Previous research by Krishnan et al. [19] has indicated that a high Taylor Factor mismatch contributes to spallation and growth. However, damage begins to nucleate at higher velocities compared to the growth direction. The low-velocity damage nucleation in the growth direction samples can be explained by their overall higher Taylor Factors compared to the growth direction. The Taylor factor can indicate the spall strength of the grain based on the plasticity needed to begin void nucleation. A high Taylor Factor would suggest the grain is weaker in spall strength because it requires less plastic deformation before voids nucleate.

Wilkerson et al. [23] developed a relationship between grain size and spall strength to predict the amount of voids nucleated in a sample. They define three fracture regions: intergranular, mixed-mode, and transgranular. For the bicrystalline experiments performed in this work with 5 mm grains and spall strengths between 3 and 4 GPa, the paper states that intergranular fracture would be the primary failure mode, which matches what is seen.

Abaqus Results from Flyer-Plate Impact Simulations

Crystal plasticity simulations were performed for both the growth and punch out orientations. Two growth direction simulations were shown in Figs. 7 and 8: shot 110 and shot 112. Both used a 500 μm target and showed incipient spall at the boundary at 223.4 m/s (shot 110) and coalesced at the boundary at 232.6 m/s (shot 112). Two outputs are of interest in each of the simulations: void volume fraction, or the ratio of voids to the total volume, and von Mises stress.

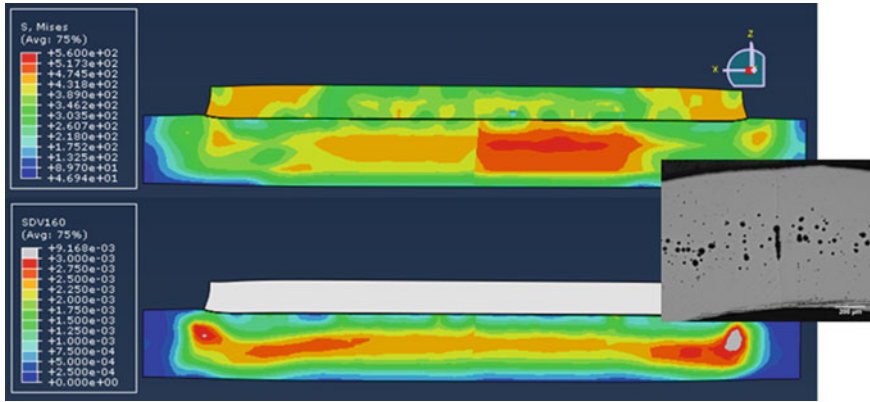


Fig. 7 Result of a 500 μm flyer with an impact of 223.4 m/s (shot 110, growth direction). Top: von Mises (MPa), bottom: void volume fraction

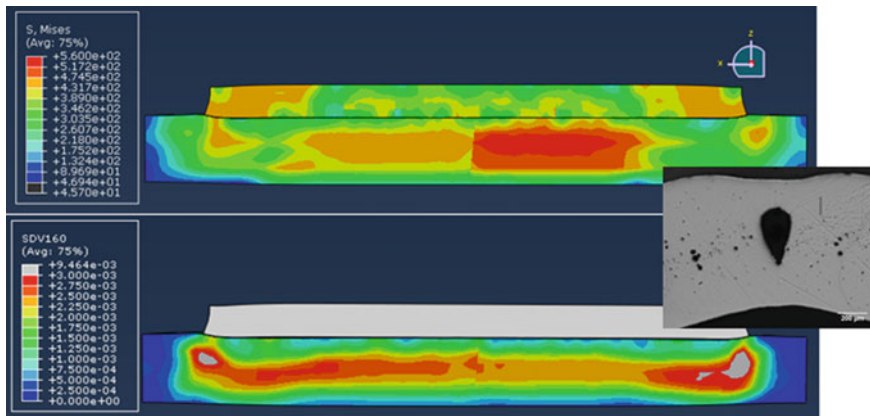


Fig. 8 Result of a 500 μm flyer with an impact of 232.6 m/s (shot 112, growth direction). Top: von Mises (MPa), bottom: void volume fraction

The void volume fraction results for both shots correlate well with each other and with experimental results. The void volume fraction is higher at the boundary for shot 112, while lower for shot 110, matching what is seen experimentally in both samples. There is also a difference in damage and stress between the bulks that can be seen in the simulations. This effect can also be seen experimentally where one grain contains voids, while the other grain fails to nucleate any voids. For the samples shown in the simulations in Figs. 7 and 8. ImageJ was used to count the voids in the bulks. The left bulk had a lower number of voids in each sample with 105 for shot 110 and 145 for shot 112, while the right bulk contained 155 and 162, respectively. Although the difference in the void count can be relatively small, this could be related to the difference in the Taylor factor between the two grains. If one grain requires

less stress to nucleate damage, voids will have a longer time to nucleate and grow compared to the grain at a higher initial stress. Further work in this area is needed to be able to confirm the orientation and Taylor Factor of each bulk in the sample to the simulation.

Conclusions

Results from the flyer-plate impact tests show clearly that the kinetics of damage growth along the boundary is strongly affected by stress level and pulse duration, and the damage kinetics increase faster at the boundary than at the bulk of the grains. Comparisons of the boundary damage between both targets show the effect of grain orientations. The punch out direction seems to need a higher stress and velocity to nucleate voids compared to the growth direction, but fast kinetics once the voids nucleate. Since the misorientation angle across the boundary was controlled, another conclusion is that void nucleation and growth at the boundary is independent of orientation. Abaqus simulations are in agreement with experimental results. Simulation results indicate a difference in von Mises stress between the two bulks, which may be linked to their respective Taylor Factors, causing the differences in bulk damage seen experimentally.

References

1. Meyers MA (1994) *Dynamic behavior of materials*. Wiley, New York
2. Minich RW, Cazamias JU, Kumar M, Schwartz AJ (2004) Effect of microstructural length scales on spall behavior of copper. *Metall Mater Trans A* 35A(9):2663–2673
3. Koller DD, Hixson RS, Gray GT III, Rigg PA, Addessio LB, Cerreta EK, Maestas JD, Yablinsky CA (2005) Influence of shock-wave profile shape on dynamically induced damage in high-purity copper. *J Appl Phys* 98:103518-1–103518-7. <https://doi.org/10.1063/1.2128493>
4. Buchar J, Elices M, Cortez R (1991) The influence of grain size on the spall fracture of copper. *J Phys IV Col 1(C3):C3-623–C3-630*. <https://doi.org/10.1051/jp4:1991387>
5. Peralta P, DiGiacomo S, Hashemian S, Luo SN, Paisley D, Dickerson R, Loomis E, Byler D, McClellan KJ, D'Armas H (2008) Characterization of incipient spall damage in shocked copper multicrystals. *Int J Damage Mech* 18:393–413. <https://doi.org/10.1177/1056789508097550>
6. Wayne L (2009) Three-dimensional characterization of spall damage at microstructural weak links in shock-loaded copper polycrystals. Master's thesis, Arizona State University
7. Cerreta EK, Escobedo JP, Perez-Bergquist A, Koller DD, Trujillo CP, Gray GT III, Brandl C, Germann TC (2012) Early stage dynamic damage and the role of grain boundary type. *Scripta Mater* 66:638–641. <https://doi.org/10.1016/j.scriptamat.2012.01.051>
8. Escobedo JP, Dennis-Koller D, Cerreta EK, Patterson BM, Bronkhorst CA, Hansen BL, Tonks D, Lebensohn RA (2011) Effects of grain size and boundary structure on the dynamic tensile response of copper. *J Appl Phys* 110:033513-1–033513-13. <https://doi.org/10.1063/1.3607294>
9. An Q, Han WZ, Luo SN, Germann TC, Tonks DL, Goddard WA III (2012) Left-right loading dependence of shock response of (111)/(112) Cu bicrystals: deformation and spallation. *J Appl Phys* 111(5):053525-1–053525-4. <https://doi.org/10.1063/1.3692079>

10. Wayne L, Krishnan K, DiGiacomo S, Kovvali N, Peralta P, Luo SN, Greenfield S, Byler D, Paisley D, McClellan KJ, Koskelo A, Dickerson R (2010) Statistics of weak grain boundaries for spall damage in polycrystalline copper. *Scripta Mater* 63:1065–1068. <https://doi.org/10.1016/j.scriptamat.2010.08.003>
11. Brown A (2014) Three dimensional characterization of microstructural effects on spall damage in shocked polycrystalline copper. Ph.D. thesis, Arizona State University
12. Brown A, Wayne L, Pham Q, Krishnan K, Peralta P, Luo SN, Patterson BM, Greenfield S, Byler D, McClellan KJ, Koskelo A, Dickerson R, Xiao X (2015) Microstructural effects on damage nucleation in shock-loaded polycrystalline copper. *Metall Mater Trans A* 46(10):4539–4547. <https://doi.org/10.1007/s11661-014-2482-z>
13. Escobedo JP, Cerreta EK, Dennis-Koller D (2013) Effect of crystalline structure on intergranular failure during shock loading. *JOM* 66(1):156–164. <https://doi.org/10.1007/s11837-013-0798-6>
14. Gray GT III, Bourne NK, Henrie BL (2007) On the influence of loading profile upon the tensile failure of stainless steel. *J Appl Phys* 101:093507-1–093507-9. <https://doi.org/10.1063/1.2720099>
15. Gray III GT, Bourne NK, Livescu V, Trujillo CP, MacDonald S, Withers P (2014) The influence of shock-loading path on the spallation response of Ta. Paper presented at the 18th APS-shock compression of condensed matter and 24th International Association for the Advancement of High Pressure Science and Technology, Seattle, WA, 7–12 July 2013. *J Phys Conf Ser* 500(11). <https://doi.org/10.1088/1742-6596/500/11/112031>
16. Rudd RE, Belak JF (2002) Void nucleation and associated plasticity in dynamic fracture of polycrystalline copper: an atomistic simulation. *Comput Mater Sci* 24:148–153. [https://doi.org/10.1016/S0927-0256\(02\)00181-7](https://doi.org/10.1016/S0927-0256(02)00181-7)
17. Wilkerson JW, Ramesh KT (2014) A dynamic void growth model governed by dislocation kinetics. *J Mech Phys Solids* 70:262–280. <https://doi.org/10.1016/j.jmps.2014.05.018>
18. Chen GS, Aimone PR, Gao M, Miller CD, Wei RP (1997) Growth of nickel-base superalloy bicrystals by the seeding technique with a modified Bridgman method. *J Cryst Growth* 179:635–646. [https://doi.org/10.1016/S0022-0248\(97\)00134-6](https://doi.org/10.1016/S0022-0248(97)00134-6)
19. Krishnan K, Brown A, Wayne L, Vo J, Opie S, Lim H, Peralta P, Luo SN, Byler D, McClellan KJ, Koskelo A, Dickerson R (2015) Three-dimensional characterization and modeling of microstructural weak links for spall damage. *Metall Mater Trans A* 46(10):4527–4538. <https://doi.org/10.1007/s11661-014-2667-5>
20. Potirniche G, Horstemeyer M (2007) An internal state variable damage model in crystal plasticity. *Mech Mater* 39:941–952. <https://doi.org/10.1016/j.mechmat.2007.04.004>
21. Bammann DJ, Aifantis EC (1989) A damage model for ductile metals. *Nucl Eng Des* 116:355–362. [https://doi.org/10.1016/0029-5493\(89\)90095-2](https://doi.org/10.1016/0029-5493(89)90095-2)
22. Liu B, Li Z, Xu F, Kikuchi M (2011) Influence and sensitivity of inertial effect on void growth and behavior in ductile metals. In: Ariffin AK, Abdullah S, Ali A, Muchtar A, Ghazali MJ, Sajuri Z (eds) *Key Eng Mater* 462–463:449–454. <https://doi.org/10.4028/www.scientific.net/KEM.462-463.449>
23. Wilkerson JW, Ramesh KT (2016) Unraveling the anomalous grain size dependence of cavitation. *Phys Rev Lett* 117(21):215503-1–215503-5. <https://doi.org/10.1103/physrevlett.117.215503>